# Polarization-oriented LiNbO3 nanocrystals by femtosecond laser irradiation in LiO2–Nb2O5–SiO2–B2O3 glasses

Research Article | Vol. 11, No. 4 / 1 April 2021 / Optical Materials Express 1313
Optical Materials EXPRESS

# Polarization-oriented $LiNbO_3$ nanocrystals by femtosecond laser irradiation in $LiO_2$–$Nb_2O_5$–$SiO_2$–$B_2O_3$ glasses

ELISA MUZI,[1,2,*] MAXIME CAVILLON,[1] MATTHIEU LANCRY,[1] FRANÇOIS BRISSET,[1] BENJAMIN SAPALY,[1] DAVIDE JANNER,[2] AND BERTRAND POUMELLEC[1]

[1] *Institut de Chimie Moléculaire et des Matériaux d'Orsay (ICMMO), Université Paris-Saclay, CNRS, 91405 Orsay, France*
[2] *Department of Applied Science and Technology (DISAT), Politecnico di Torino, 10129 Torino, Italy*
[*] *elisa.muzi@universite-paris-saclay.fr*

**Abstract:** This work investigates the role of a $B_2O_3$ addition (up to 21 mole %) into a lithium niobium silicate glass matrix, focusing on the orientational dependency of second harmonic generation (SHG), induced after femtosecond laser irradiation. We detected the sharp emission of light at 515 nm, characteristic of SHG, in both static and scanning configurations, using pulse energy, repetition rate, and laser polarization as varying parameters. Among the results to highlight, the SHG signature appears within a few seconds in highly doped $B_2O_3$ glass, i.e., one order of magnitude smaller than in $B_2O_3$-free glass. Additionally, we found that the orientability of the polar axis of $LiNbO_3$ nanocrystals by writing laser polarization can be obtained in glasses when $SiO_2$ is substituted with $B_2O_3$. These preliminary results open the door to the fabrication of crystal / glass based photonic devices with lower laser power deposited and much faster crystallization kinetics.



## 1. Introduction

Femtosecond (fs) laser direct writing (FLDW) is a powerful and versatile tool enabling a large variety of optical components to be fabricated in transparent materials such as glasses (e.g. Bragg gratings, waveguides, graded index lenses, birefringent optics) [1–3]. In addition to surface modifications, the femtosecond laser irradiation has allowed the 3D-nanostructuring of optical properties induced by permanent effects on material structure. By controlling the fs-laser parameters (e.g. pulse energy, repetition rate, scanning speed, polarization), it becomes possible to induce crystallization inside a glass substrate with a high spatial selectivity (few tens of $\mu m^3$ or less). Some examples of crystals induced by FLDW in glasses can be found in the recent review of Komatsu et al. [4], among which we can cite $\beta$-$BaB_2O_4$ [5], $Ba_2TiSi_2O_8$ [6], or $LiNbO_3$ [7].

A particular focus is about fs-laser crystallization of $LiNbO_3$ in silicate matrix, a crystal that allows many applications in different fields because of its properties: ferroelectricity, pyroelectricity, piezoelectricity and a large second order susceptibility. In particular, because of its axial symmetry, the second order susceptibility tensor ($\chi^{(2)}$) of $LiNbO_3$ crystal is such that its nonlinear coefficient value along the polar axis ($d_{33}$ = 34.4 pm/V [8,9]) is much greater than the nonlinear coefficients values along the other axes ($d_{31}$ = 4.88 pm/V, $d_{22}$=2.58 pm/V [8,9]). Therefore, it presents an angular dependence of $\chi^{(2)}$-related processes, such as second harmonic generation (SHG). This translates into a modulation of the SHG signal during FLDW that occurs when the crystals can be oriented along the direction of laser polarization.

To produce crystallization by FLDW, the typical glass matrix used in previous works is composed of 33%$Li_2O$ – 33%$Nb_2O_5$ – 34%$SiO_2$ (LNS) (molar %) [7,10]. Although interesting results have been published, the impact of the glass matrix has not been studied extensively yet.

#417461 https://doi.org/10.1364/OME.417461
Journal © 2021 Received 11 Dec 2020; revised 11 Feb 2021; accepted 24 Feb 2021; published 31 Mar 2021

Optical Materials EXPRESS

In particular, if $SiO_2$ is partially substituted with $B_2O_3$, the impact on the crystallization rate can drastically increase, unlocking in such a way the industrial potential of this direct writing technique. Indeed, the incorporation of $B_2O_3$ into the glass matrix is of interest as it is expected to lower the glass transition temperature and, thus, to improve the kinetics of $LiNbO_3$ crystallization compared for LNS glass [11–14].

In this work, we report on the impact of $LiNbO_3$ crystallization by FLDW by adding a significant amount of $B_2O_3$ in the glass matrix (through modification of the starting glass batch composition). We revealed the creation of polarization dependent $\chi^{(2)}$ by the SHG detection and confirmed this is related to $LiNbO_3$ nanocrystals by electron backscattered diffraction (EBSD) measurements. As a reference, we start with the crystallization of a typical LNS glass. We, then, intend to analyze the impact on fs-laser irradiation on glass crystallization, when $SiO_2$ is partly substituted with $B_2O_3$. More specifically, we aim at determining whether it is possible to induce tunable SHG angular modulation in these glassy matrices and to identify the orientation of the laser-induced nanocrystals in these borosilicate glass matrices compared to LNS glass (i.e., $B_2O_3$-free glass).

## 2. Method

Four glasses, with increasing $B_2O_3$ content up to 21%, were fabricated using melt-quenching technique. Compositions and labels are reported in the Table 1. A powder mixture of 30 grams per batch composed of $SiO_2$ (99.9%, SERLABO), $H_3BO_3$ (99.5%, PROLABO), $Li_2CO_3$ (99.9%, SIGMA ACS reagent) and $Nb_2O_5$ (99.5%, STREM CHEMICALS) powders in stoichiometric amount, was first homogenized using acetone. The mixed powder was then placed inside a platinum crucible and dried at 200°C for 2 hours before increasing the temperature at a heating rate of 5°C/min up to 1000°C. The mixed powder remained at this temperature for 1 hour. After that, to obtain the melting, the temperature was increased to 1400°C for LNS34 and 1350°C for LNS27B7, LNS20B14, LNS13B21 at a heating rate of 10°C/min. Finally, the molten mixture was quenched between two metal plates preheated at around 350°C and maintained at this temperature for about 30 minutes.

**Table 1. Glass labels and batch compositions**

| Glass label | Glass batch composition (mol%) |
|---|---|
| **LNS34** | 33% $LiO_2$ – 33% $Nb_2O_5$ – 34% $SiO_2$ |
| **LNS27B7** | 33% $LiO_2$ – 33% $Nb_2O_5$ – 27% $SiO_2$ – 7% $B_2O_3$ |
| **LNS20B14** | 33% $LiO_2$ – 33% $Nb_2O_5$ – 20% $SiO_2$ – 14% $B_2O_3$ |
| **LNS13B21** | 33% $LiO_2$ – 33% $Nb_2O_5$ – 13% $SiO_2$ – 21% $B_2O_3$ |

The obtained glasses had the shape of a slab of about 1 mm thickness. For laser irradiation, samples were double side polished to reach optical quality and then they were placed on the FLDW system that comprises a motorized translation stage and a commercial femtosecond laser (Satsuma, Amplitude Systèmes Ldt, $\lambda = 1030$ nm, pulse duration = 250 fs). Each irradiation was performed by focusing the laser beam approximately 240 µm below the sample top surface using a 0.6 numerical aperture (NA) aspheric lens. We choose this focusing depth to avoid any surface ablation when scanning over long distances and to avoid heterogenous nucleation preferentially triggered at the surface.

The translation stage enables a displacement in the XY plane, while the laser beam propagation direction is along the Z direction as depicted in Fig. 1(a). Three different laser polarization configurations referenced relative to the laser writing direction, along the Y-axis, were used: parallel: parallel ($Y_y$), at 45° ($Y_{45}$) and perpendicular ($Y_x$) to it. The SHG intensity was recorded in transmission using a spectrometer (Jaz, Ocean Optics) equipped with a multimode optical fiber

Optical Materials EXPRESS

and a coupling lens to maximize light collection from the sample. A more detailed description of the setup is reported in Ref. [7].

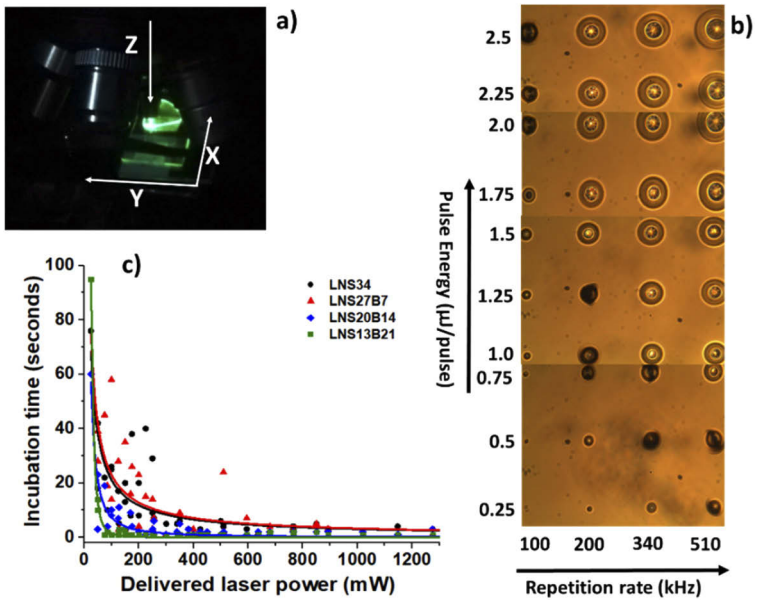


**Fig. 1.** a) Typical image of SHG detected after few seconds under static irradiation that corresponds to the end of the incubation time; b) Optical microscope image in transmission and white light of static irradiation until the onset of SHG of LNS34 glass sample with varying laser parameters; c) Incubation time as a function of the power (in mW) delivered by the laser in static conditions for four glass compositions. Laser conditions used: $\lambda = 1030$ nm, NA = 0.6, f = 200 kHz, focus depth = 240 µm in air. In Fig. 1(c), each data set was fitted with a power law ($ax^b$); the latter only serves as a guide-to-the-eye.

We started by performing a static irradiation to investigate the influence of laser parameters during laser-induced crystallization. This experiment, carried out on each sample, served to determine the incubation time as a function of glass composition. The incubation time is the time taken, upon fs-laser irradiation, until the observation of the SHG signal ($\lambda_{SHG} = \lambda/2 = 515$ nm) and is indicative of the early birth of non-centrosymmetric crystals, typically $LiNbO_3$ is expected in our case [7]. At this stage, only two laser parameters were varied, i.e., the pulse energy, ranging from 0.25 to 2.5 µJ, in steps of 0.25 µJ and the laser repetition rate, with values of 100 kHz, 200 kHz, 340 kHz, and 510 kHz. The laser polarization was fixed along the X-axis that is defined by the plane of laser compressor. The minimum incubation time to induce crystallization, found from the above experiments, is also needed for writing lines structures. First the laser was set in static mode for the minimum incubation time until green light was detected; then the laser scanning was started. Line writing parameters were set at a fixed repetition rate of 200 kHz and writing speed of 1 µm/s using different pulse energies (0.25 µJ to 2.0 µJ, step of 0.25 µJ). This was repeated for the three different laser polarization configurations to assess their influence on the crystal orientation, namely parallel ($Y_y$), at 45° ($Y_{45}$) and perpendicular ($Y_x$).

For each written line, we measured the SHG intensity in the XY plane according to the azimuthal angle (θ) of the probe beam polarization, up to 180° starting from the polarizer reference position in correspondence of 0°, i.e., along X. The probe beam propagation direction was set perpendicular to the XY plane and its electric field direction was parallel to this plane.

In our samples, the SHG intensity was measured in transmission mode with the fundamental beam (1030 nm) propagating perpendicularly to the sample XY plane at pulse energy = 0.1 µJ/pulse.

Optical Materials EXPRESS

The spot size (diameter) of the probing beam was approximately 30 μm, well overlapping each laser track during SHG measurements. The repetition rate during the measurement was set at 100 kHz. The transmitted SHG light (515 nm) was recorded after passing an IR low pass filter mounted before the spectrometer collector.

Finally, to investigate the correlation between the laser induced microstructure and the SHG response, we proceeded with an analysis at field-emission scanning electron microscope (FEG-SEM ZEISS SUPRA 55 VP) with electron backscattered diffraction (EBSD) detector (TSL-EDAX Velocity Camera and OIM Analysis software).

## 3. Results and discussion

In Fig. 1, we report respectively: a) the SHG signal detected upon irradiation, b) the laser induced modifications observation under optical microscope with varying conditions, and c) incubation times measured for each glass sample under static irradiation. In particular, Fig. 1(b) illustrates the dependence of the laser affected zone on both pulse energy ($E_p$) and repetition rate ($RR$). As the deposited power ($P = RR$ x $E_p$) increases, the area of the modified region becomes wider than the spot size, which is characteristic of thermal accumulation in and around the focal spot (of radius $w_0 \sim 1.2\lambda/(2NA) \sim 1$ μm). Figure 1(c) shows that the measured incubation time decreases as the delivered power $P$ increases. For similar experimental conditions, these measurements clearly indicate the tendency for LNS13B21 glass to crystallize at a much higher rate compared to other glasses. For example, at a delivered power of 100 mW, LNS13B21 sample exhibits an incubation time of ~1 second, while it is of ~10 seconds for LNS20B14 and ~20 seconds for both LNS27B7 and LNS34, as represented in Fig. 1(c). In term of laser-affected volume, we observe that both laser track width and length (measured within the cross section) increase along with the pulse energy. This behavior is characteristic of more heat deposited inside the glass upon irradiation and it is in agreement with results from Fig. 11 in Ref. [7].

To assess the effect of the orientation of the writing laser polarization on the crystals, we investigated the angular dependency of the SHG intensity. All the measured values, as a function of the azimuthal orientation of the probing linear polarization, were normalized relative to their highest value as shown in Fig. 2. Here we compared two writing configuration schemes: $Y_x$ and $Y_{45}$. In particular, we choose to represent those relative to two characteristics pulse energies, i.e., 0.5 μJ and 1.25 μJ, because of important SHG trends variations that are visible in Fig. 2(a) and 2(b), for the four investigated glasses. For the lowest energy value, a strong SHG modulation is found with an azimuth-$\theta$ of 90° for all glasses. For pulse energy of 1.25 μJ, the evidence of SHG "directionality" is strongly reduced for all four samples, as it is more easily visible from the polar representations referring to LNS1B21 sample, reported in Fig. 2(c). Here we note the occurrence of a second maximum on the SHG ($\theta$) curve along the polarization direction.

More specifically, from Fig. 2, we observe that at the lowest energy (0.5 μJ/pulse), the normalized SHG intensity ($I/I_{max}$) follows a sinusoidal behavior with a strong contrast ($I_{max}$-$I_{min}$)/($I_{max}$+$I_{min}$) up to 0.9 for LNS20B14. We note a maximum for a direction perpendicular to the laser polarization i.e., 90° and 135° for $Y_x$ and $Y_{45}$ configurations, respectively. In contrast the minimum SHG is found for a probing angle perpendicular to the maximum one. This is in agreement with Ref. [10], where the polar axis of $LiNbO_3$ is oriented perpendicularly to the laser polarization. Interestingly, this behavior is preserved even after a large substitution of $SiO_2$ with $B_2O_3$.

As the pulse energy is increased, from 0.5 to 1.25 μJ, the SHG intensity profile becomes more "isotropic", which could be caused by the presence of several crystalline textures with different orientations [15]. Indeed, from Fig. 2(c) we can see that the low energy texture (population leading to $SHG_{max}$ for $\theta$ perpendicular to writing polarization) is still appearing at 1.25 μJ. However, there is another contribution that appears in the SHG ($\theta$) response, and is indicative of a second texture (i.e., a second population of $LiNbO_3$ crystals with a preferential orientation).

Optical Materials EXPRESS

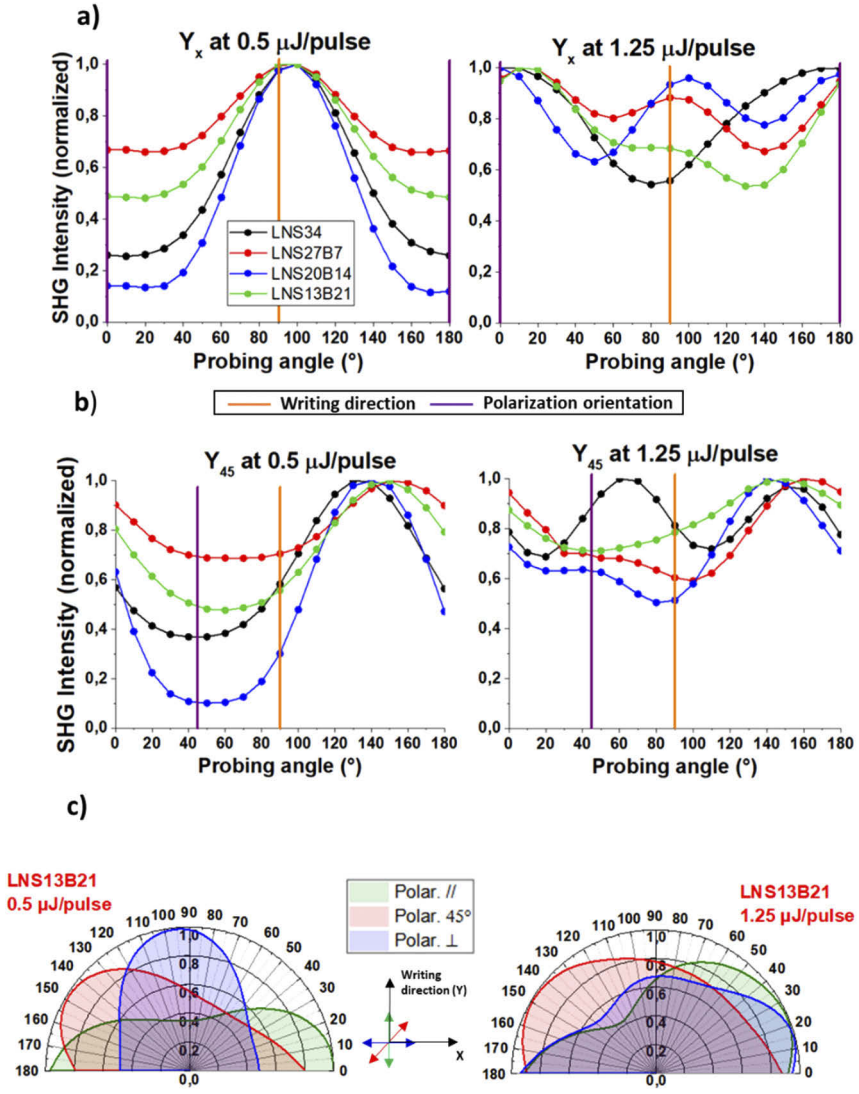


**Fig. 2.** Normalized SHG intensity for four glass compositions as a function of probing polarization angle in the XY plane as defined in the text, a) for the four glass samples, configuration $Y_x$ at two pulse energies: 0.5 µJ/pulse and 1.25 µJ/pulse; b) same as a) but for the $Y_{45}$ configuration. Both the writing direction and the laser polarization during writing are reported on each graph; c) polar representations for LNS13B21 glass for 0.5 µJ/pulse and 1.25 µJ/pulse with three configurations: $Y_y$, $Y_{45}$ and $Y_x$ (the polarization orientations with respect to writing direction are indicated by double headed arrows in the coordinates of the reference system).

Optical Materials EXPRESS

This is also clear with the configuration $Y_{45}$ for which there is no maximum in the direction of writing.

One could expect the minima and maxima of the SHG modulation to be positioned exactly 90° apart from the laser polarization. However, a slight departure from this angle is observed, and

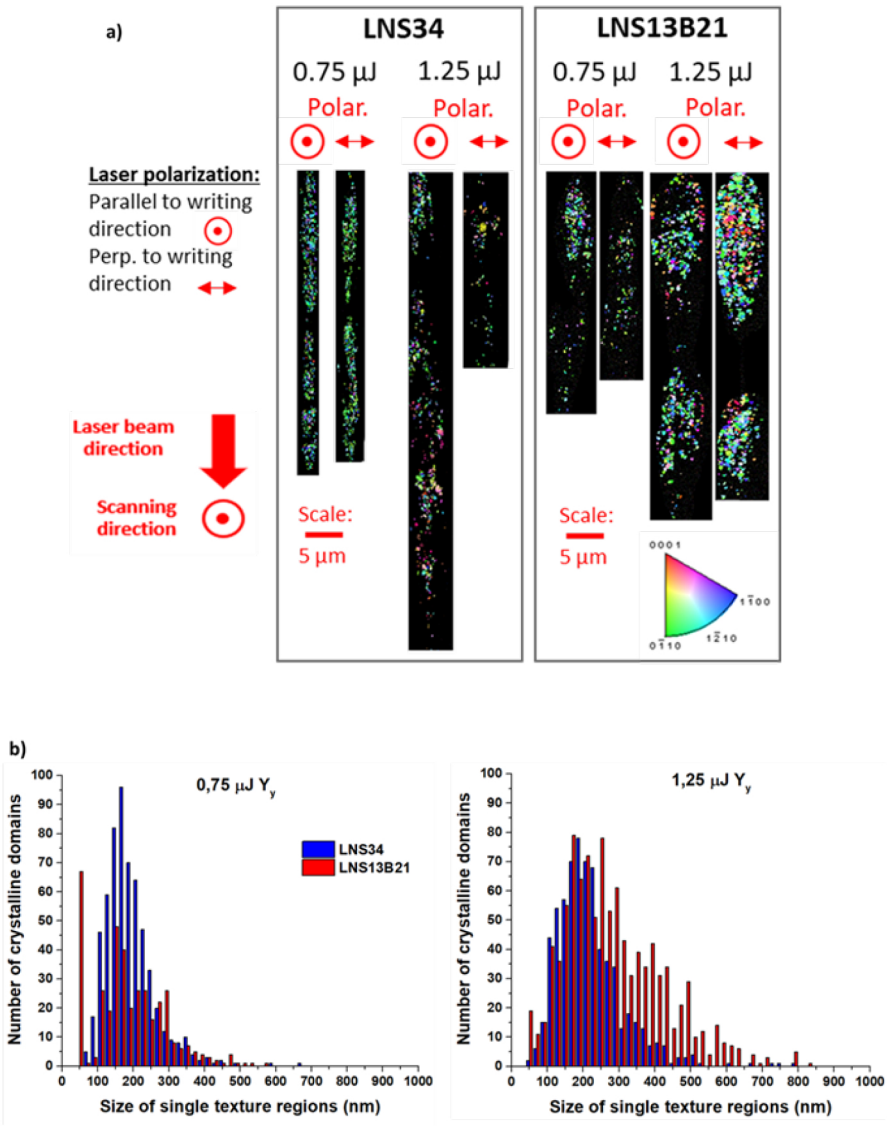


**Fig. 3.** a) Electron Back Scatter Diffraction (EBSD) micrographs of the laser track cross sections for both LNS34 and LNS13B21 glass samples, for two pulse energies (0.75 µJ/pulse and 1.25 µJ/pulse) and with laser polarization either parallel or perpendicular to the scanning direction. The inverse pole figure (IPF) color code is based on $LiNbO_3$ space group, with coding along the laser polarization direction; b) Size distribution of single texture regions for LNS34 and LNS13B21 for the $Y_y$ configuration and two different pulse energies (0.75 µJ and 1.25 µJ). Irradiation conditions: $\lambda = 1030$ nm, NA = 0.6, f = 200 kHz, focus depth = 240 µm in air, writing speed = 1 µm/s.

Optical Materials EXPRESS

may be due to an asymmetric orientational writing effect as previously observed at low speeds (1 µm/s, similar to this work) in LNS glass [15].

Finally, to validate the presence of the $LiNbO_3$ crystals and to study their orientation inside the laser track cross sections, electron backscattered diffraction (EBSD) analysis was performed on LNS34 and LNS13B21 samples [16,17]. The results are presented in Fig. 3(a).

We first observed that $LiNbO_3$ nanocrystals were effectively precipitated. Secondly, from the inverse pole figure (IPF) color code, the crystal c axis (along the 0001 direction) is found to be oriented perpendicular to the laser polarization (absence of red color on the EBSD map).

This is obviously the case at the lowest pulse energy, whereas at higher energies crystal c axis orientation is observed to vary and be only partially oriented along the polarization direction. Note that these observations are in agreement with the SHG experiments: at low pulse energies the crystals are well oriented with their c axis perpendicular to the writing laser polarization and corresponding to a maximum SHG contrast with a nearly single texturation. However, at higher pulse energies, a part of the nanocrystals population exhibit c axis orientation along the polarization leading to a more spatially distributed (hence isotropic) SHG response.

From the EBSD data (Fig. 3(a)) we could distribution of single texture regions of nanocrystals (assuming they are spherical) within the investigated laser track area. In Fig. 3(b), we report this distribution for LNS34 and LNS13B21 for the $Y_y$ configuration and two different pulse energies (0.75 µJ and 1.25 µJ). At the highest pulse energy (1.25 µJ in this comparison) we observe the tendency to form larger regions with same textures compared to the low energy conditions (0.75 µJ, 20 nm – 300 nm diameter range).

## 4. Conclusion

In this work, we demonstrated that tunability of SHG in lithium niobate silicate glass can be extended to the borosilicate glass family, through an adequate control of the laser parameters. More specifically, the substitution of $SiO_2$ with $B_2O_3$ is found to be advantageous as it promotes faster crystallization of $LiNbO_3$ crystals while preserving the tunability of SHG. The latter is related to the larger SHG response along the c axis of the crystals, which is preferentially aligned perpendicular to the laser polarization at low pulse energy. Currently, the $LiNbO_3$ orientation is understood as being due to alignment of the larger linear susceptibility matrix element ($\perp$ to c axis) with the electric field [18]. We also observe that LNS13B21 glass exhibits a shorter incubation time and thus likely a faster crystal growth with respect to LNS34 that may explain the larger crystals at 1.25 µJ, and more experiments are ongoing to confirm this hypothesis. Several key properties of the written structures related to photonic devices fabrication will be investigated in the future, including refractive index changes and birefringence response.

**Funding.** Compagnia di San Paolo (Joint Research Program); Agence Nationale de la Recherche (CHARMMMAT ANR-11-LABX-0039).

**Acknowledgments.** This work was supported by the French National Research Agency under the program CHARMMMAT ANR-11-LABX-0039-grant. Elisa Muzi and Davide Janner also acknowledge financial support from Compagnia di S. Paolo through the Joint Research Program.

**Disclosures.** The authors declare no conflicts of interest.

## References

1. R. R. Gattass and E. Mazur, "Femtosecond laser micromachining in transparent materials," Nat. Photonics **2**(4), 219–225 (2008).
2. J. Habel, T. Boilard, J. S. Freniere, F. Trepanier, and M. Bernier, "Femtosecond FBG written through the coating for sensing applications," Sensors **17**(11), 2519 (2017).
3. T. T. Fernandez, M. Sakakura, S. M. Eaton, B. Sotillo, J. Siegel, J. Solis, Y. Shimotsuma, and K. Miura, "Bespoke photonic devices using ultrafast laser driven ion migration in glasses," Prog. Mater. Sci. **94**, 68–113 (2018).
4. T. Komatsu and T. Honma, "Laser patterning and growth mechanism of orientation designed crystals in oxide glasses: A review," J. Solid State Chem. **275**, 210–222 (2019).

Optical Materials EXPRESS


5. K. Miura, J. Qiu, T. Mitsuyu, and K. Hirao, "Space-selective growth of frequency-conversion crystals in glasses with ultrashort infrared laser pulses," Opt. Lett. **25**(6), 408–410 (2000).
6. B. Zhu, Y. Dai, H. Ma, S. Zhang, G. Lin, and J. Qiu, "Femtosecond laser induced space-selective precipitation of nonlinear optical crystals in rare-earth-doped glasses," Opt. Express **15**(10), 6069–6074 (2007).
7. J. Cao, M. Lancry, F. Brisset, L. Mazerolles, R. Saint-Martin, and B. Poumellec, "Femtosecond laser-induced crystallization in glasses: growth dynamics for orientable nanostructure and nanocrystallization," Cryst. Growth Des. **19**(4), 2189–2205 (2019).
8. M. J. Weber, ed., *CRC Handbook of Laser Science and Technology* (CRC Press, 1986), Vol. Optical materials, Part 1: Nonlinear Optical Properties/Radiation damage.
9. R. S. Klein, G. E. Kugel, A. Maillard, and K. Polgar, "Considerations of angular acceptance and non- linear optical coefficient measurements by second harmonic generation in $LiNbO_3$ crystals," Ferroelectrics **296**(1), 57–66 (2003).
10. J. Cao, L. Mazerolles, M. Lancry, F. Brisset, and B. Poumellec, "Modifications in lithium niobium silicate glass by femtosecond laser direct writing: morphology, crystallization, and nanostructure," J. Opt. Soc. Am. B **34**(1), 160–168 (2017).
11. M. P. Fernandes Graca and M. Almeida, "Glass ceramics with para, anti or ferroelectric active phases", in *Advances in Ceramics - Electric and Magnetic Ceramics, Bioceramics, Ceramics and Environment* (IntechOpen, 2011).
12. A. Faeghi-Nia, V. K. Marghussian, and E. Taheri-Nassaj, "Effect of $B_2O_3$ on crystallization behavior and microstructure of $MgO–SiO_2–Al_2O_3–K_2O–F$ glass–ceramics," Ceram. Int. **33**(5), 773–778 (2007).
13. G. Ferlat, A. P. Seitsonen, M. Lazzeri, and F. Mauri, "Hidden polymorphs drive vitrification in $B_2O_3$," Nat. Mater. **11**(11), 925–929 (2012).
14. W. Vogel, *Glass Chemistry* (Springer-Verlag, 1994).
15. J. Cao, B. Poumellec, F. Brisset, A. L. Helbert, and M. Lancry, "Angular dependence of the second harmonic generation induced by femtosecond laser irradiation in silica-based glasses: variation with writing speed and pulse energy," World J. Nano Sci. Eng. **05**(03), 96–106 (2015).
16. B. Poumellec, M. Lancry, C. Fan, A. Erraji-Chahid, and P. Kazansky, "Asymmetric orientational femtosecond laser writing detected in several properties in various glasses," Advances in Optical Materials, OSA Technical Digest (CD) (Optical Society of America, 2011), paper AIFB2.
17. K. Veenhuizen, D. N. Sean McAnany, B. Aitken, V. Dierolf, and H. Jain, "Fabrication of graded index single crystal in glass," Sci. Rep. **7**(1), 44327 (2017).
18. J. Cao, B. Poumellec, F. Brisset, A.-L. Helbert, and M. Lancry, "Tunable angular-dependent second- harmonic generation in glass by controlling femtosecond laser polarization," J. Opt. Soc. Am. B **33**(4), 741–747 (2016).